ni

COMPUTER SOLUTIONS OF THE GRAVITATIONAL N-BODY PROBLEM

By Frank Hohl

NASA Langley Research Center
Langley Station, Hampton, Va.

Presented at the International Astronomical Union Colloquium on the Gravitational Problem of N Bodies

Paris, France
August 16-18, 1967

COMPUTER SOLUTIONS OF THE GRAVITATIONAL N-BODY PROBLEM

By Frank Hohl

NASA Langley Research Center

Thermalization effects in a one-dimensional model for a self-gravitating system have been investigated for systems containing low numbers of mass sheets (up to 40). It is found that the fluctuation of the kinetic energy is inversely proportional to the square root of the number of particles in the system.

The stability of stationary states for one-dimensional self-gravitating systems is investigated by solving the N-body problem on an electronic computer. The number of "stars" in such systems is large (several 1000) so that the systems can be treated as collisionless. A variational method is used to show that stationary distribution functions that are always decreasing in going outward from the center of the system are stable. For other stationary distributions the system does not represent a minimum energy configuration and the system may be unstable. Computer solutions illustrating the resulting instabilities are presented.

Numerical experiments with a simple two-dimensional rod model show that the spiral structure and other filamentary structure of galaxies may result from purely gravitational effects.

THERMALIZATION EFFECTS IN A ONE-DIMENSIONAL STELLAR SYSTEM

In a one-dimensional system crossings will always take place so that one can expect the system to approach a Maxwellian distribution. An exact double-precision computer program was used to investigate thermalization effects for low numbers of "stars." By an "exact" program we refer to a program where the

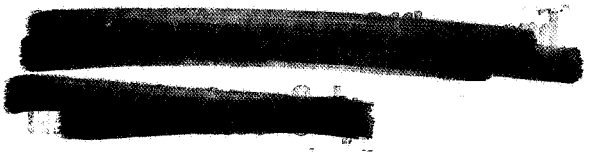

shortest crossing time for a mass sheet is determined and the system is then advanced by that time and the process is repeated. This, of course, differs from the model used for the results obtained for systems with large numbers of mass sheets where the system is always advanced for a constant time interval Δt, irrespective of the number of crossings during this time interval. The "exact" program is very accurate. For example, after time reversing the numerical integration of a typical system investigated it was found that the initial conditions were reproduced accurately to 12 digits.

The relaxation or characteristic time for a system of stars is given by

$$\tau_c = (4\pi G\rho)^{-1/2} \tag{1}$$

where G is the gravitational constant and ρ is the mass density. The characteristic length of interest is the Jeans or Debye length D which is defined by

$$D = V_T \tau_c \tag{2}$$

where V_T is the velocity dispersion of the system of stars.

Lecar (ref. 1) has investigated the exact one-dimensional motion of low numbers of "stars" and finds that to order $nD\tau_c$ there exists no thermalization. In the present study of thermalization effects a low number of mass sheets was chosen so that the system can be followed for a long period of time. In order to obtain meaningful results time averages of the systems are investigated. The constant time interval used in the averaging process is taken to be smaller than the average crossing time for sheets in the system. The time averages are taken over times of the order $n^2D^2\tau_c$ where $nD \sim N$, the number of mass sheets in the system. It should be noted that the investigation of

thermalization effects is still in progress and only some of the initial numerical results are presented here.

For all of the systems investigated it was found that the time-averaged potential energy (P) and kinetic energy (T) satisfied the virial theorem. That is, $\langle T \rangle / \langle P \rangle = 0.5$ with an accuracy of at least three digits. The $\langle\ \rangle$ signify time-averaged quantities. As discussed by Ford (ref. 2) the Poincare recurrence time and the general behavior of the system is dependent on the initial conditions. For example, we can choose special initial conditions such that the time behavior of the system is very nearly periodic. However, for the results presented here the initial conditions were arbitrarily chosen.

Figure 1 shows the time-averaged velocity distribution and density for a 3-particle system. The solid line for the velocity distribution corresponds to a Maxwellian distribution and is obtained by integrating $A \exp(-\kappa U)$ over x. That is,

$$f(v) = \frac{N}{2}\sqrt{\frac{2m\kappa}{\pi}} \exp\left[-\frac{1}{2} m\kappa v^2\right] \tag{3}$$

The solid line for the density is given by

$$n(x) = \frac{1}{2} \pi G m^2 N^2 \kappa \operatorname{sech}^2\left(\pi G m^2 N \kappa x\right) \tag{4}$$

The value of κ is obtained from

$$\kappa = \frac{3N}{2\langle T \rangle + 2\langle P \rangle} = \frac{N}{2\langle T \rangle} \tag{5}$$

The circles in figure 1 represent the time-averaged numerical results. The "experimental" velocity distribution is near the Maxwellian distribution. However, the variation of the density indicates that there is some near-periodic behavior of the system. Such near-periodic behavior is likely

to occur for very low numbers of "stars." Figure 2 shows the results for a four-sheet system. Again, the variation of the time-averaged velocity distribution and density indicates that there is near-oscillatory behavior of the system. This oscillatory behavior has also been observed by plotting the kinetic energy of the system as a function of time. The fluctuations of the kinetic energy of the systems investigated are very violent and show no decrease in time. The fact that these fluctuations show no decrease in time indicates that a Maxwellian distribution can be reached while the fluctuations in the kinetic energy remain extremely violent. For example, figure 3 shows the time variation of the kinetic energy for a 6-particle system. The corresponding time-averaged velocity distribution and density are shown in figure 4. We see that the "experimental" points are near the Maxwellian distribution for both curves. Figure 5 shows that for a 10-particle system the "experimental" velocity distribution and density points reproduce the theoretical Maxwellian curves. The results presented so far were obtained by time averaging the system over times of the order of $N^2\tau_c$ and the results indicate that the time-averaged distribution is very nearly Maxwellian. However, to show relaxation to a Maxwellian distribution one should prepare a system which is initially non-Maxwellian and then observe the relaxation to a Maxwellian distribution. This was attempted and the results for a 40-particle system are shown in figure 6. The solid line corresponds to a Maxwellian velocity distribution. The circles represent the initial velocity distribution of the system obtained by time averaging over $5N\tau_c$. After the system was advanced in time for $2N^2$ characteristic periods it was found that the experimental velocity distribution was still identical to the initial distribution. Thus one must conclude that no relaxation to a Maxwellian distribution occurs to order $N^2\tau_c$.

Another quantity which gives information on the behavior of the system is the correlation function for the kinetic energy

$$C(\tau) = \langle (T(t) - \langle T \rangle)(T(t + \tau) - \langle T \rangle) \rangle \tag{6}$$

This quantity is plotted in figure 7 for a 6-particle system and the result shows that oscillations in the kinetic energy have a long-time memory and are only slowly damped. The energy correlation function for a 40-particle system is shown in figure 8. The results indicate that for small τ there exists Landau damping but some smaller correlation persists for a long time. If the time average is taken over a longer time, then the oscillations in $C(\tau)$ are reduced for large τ and remain the same for small τ. In figure 9 the relative fluctuation of the kinetic energy

$$\mu = \frac{C(0)}{\langle T \rangle} \tag{7}$$

is plotted as a function of the number of particles N. It can be seen that the points fall near the curve $1/\sqrt{N}$ which indicates that the oscillations in the kinetic energy of the systems do represent thermal fluctuations. It is therefore difficult to explain the long-time correlation shown in figures 7 and 8.

MINIMUM ENERGY PROPERTY

It will now be shown that the minimum energy property which has been obtained by Hohl and Feix (ref. 3) for a special distribution can be extended to arbitrary distribution functions. The water-bag model illustrated in figure 10 is used in the analysis. The contours $v_+^{(k)}(x,t)$ and $v_-^{(k)}(x,t)$ describe surfaces of constant distribution function $f = f_k$. According to the Liouville theorem the phase space bounded by the contours is incompressible.

In the limit of a very large number of contours the water-bag model can be used to construct arbitrary distribution functions.

To simplify the equations we assume symmetric contours $v_+^{(k)} = v_-^{(k)} = v^{(k)}$. It is easily shown (ref. 4) that the equations which stationary contours $v^{(k)}$ must satisfy are

$$v^{(k)} \frac{dv^{(k)}}{dx} - E = 0 \tag{8}$$

E is given by

$$E(x) = 4Gm\left(\frac{N}{2} - 2\sum_k A_k \theta^{(k)}(x)\right) \tag{9}$$

where G is the gravitational constant, N is the number of mass sheets, each of mass m per unit area, in the system.

A_k is defined by the distribution function

$$f = \sum_k A_k\left[\delta_{-1}\left(v - v_-^{(k)}\right) - \delta_{-1}\left(v - v_+^{(k)}\right)\right]$$

with $\delta_{-1}(z) = \int_{-\infty}^{z} \delta(\zeta)d\zeta$. The variable $\theta^{(k)}$ used in equation (9) is

$$\theta^{(k)} = \int_{-x_s^{(k)}}^{x} v^{(k)}(\zeta)d\zeta \tag{10}$$

where $x_s^{(k)}$ is the end point of the contour k. The total energy of the system is

$$W = \sum_k \int_{-x_s^{(k)}}^{x_s^{(k)}} g\, dx$$

$$= \sum_k \int_{-x_s^{(k)}}^{x_s^{(k)}} \left\{\frac{1}{3} mA_k v^{(k)3} - 2mxA_k\left[4\pi Gm\left(\frac{N}{2} - 2\sum_k A_k\theta^{(k)}\right)\right]\right\} \tag{11}$$

Extremizing the integral for W requires that g satisfy the Euler-Lagrange equation

$$\frac{\partial g}{\partial \theta^{(k)}} - \frac{d}{dx}\left(\frac{\partial g}{\partial v^{(k)}}\right) \tag{12}$$

or

$$v^{(k)} \frac{dv^{(k)}}{dx} - E = 0 \tag{13}$$

which are the equations for the stationary contours.

If equations (13) are to represent a minimum energy configuration the Legendre's criterion of the second variation of g must be satisfied. That is, the quadratic form whose coefficient matrix has the elements

$$a_{ij} = \frac{\partial^2 g}{\partial v^{(i)} \partial v^{(j)}} \tag{14}$$

must not be negative. Since only the diagonal elements

$$a_{kk} = 2mA_k v^{(k)} \tag{15}$$

are nonzero, the Legendre condition requires that

$$A_k \geqq 0 \tag{16}$$

for all k. Equation (16) is equivalent to stating that the distribution function must always decrease in going outward from the center of the system where $f = f_1$ must be the largest. If equation (16) is satisfied, the system is a minimum energy configuration and is always stable. However, if $A_k \geqq 0$ is not satisfied for all k, the system is not a minimum energy configuration. The system may then be unstable since the contours $v^{(k)}$ can now be deformed while keeping the total system energy constant. Numerical experiments with a one-dimensional model have been performed for two-contour systems to illustrate the

interchange instability which destroys the stationary state. For the two systems investigated $A_1 = -A_2$. In the first case shown in figure 11 the ratio of the minimum to maximum star energy is 0.4. The figure shows that the stationary contours of the 2000-star system are quickly distorted while the heavier outer water bag tries to displace the inner bag. Figure 12 shows the results for a 2000-star system with a ratio of minimum to maximum star energy equal to 0.25. The growth of the instability is now much slower because the central water bag or hole is much smaller.

Another consequence of the minimum energy property is that any stable stationary state for which equation (16) is satisfied can never be reached.

TWO-DIMENSIONAL COMPUTER EXPERIMENTS FOR STELLAR SYSTEMS

The motion of mass rods that are of infinite extent in the z-direction has been computed for 500-rod systems. The force acting on a particular mass rod is obtained by summing directly over the $1/r$ force from each mass rod. This is a time-consuming process and the application of fast methods of solving the Poisson equation would speed up the calculations. A fast method of solving the Poisson equation has been used by Hockney (ref. 5) who followed the motion of 2000 mass rods. In comparing the results obtained by the two different methods it was found that they are nearly identical.

The system of mass rods is advanced in time in the following manner. First, the force acting on all particles is computed by summing the $1/r$ force for all particles. Second, the system is advanced for a small time step Δt and the process is repeated. The results of the calculations are displayed in x-y coordinate space. During the calculations the total energy and angular

momentum are computed to check on the accuracy of the computations. The normalizations $4\pi G = 1$ and $m = 1$ have been used for all the calculations.

Figure 13 shows the time development of a system of 400 mass rods which has an initially rectangular distribution of uniform density in x-y space. The system has an initial thermal energy equal to 1/5 of the initial potential energy plus an initial solid-body rotation equal to nearly twice that required to oppose the gravitational force toward the center of the system. It can be seen from figure 13 that the system quickly develops into a barred spiral. However, at a later time the spiral structure has almost completely disappeared and the system approaches a configuration similar to an elliptical galaxy. The time has been normalized to ω_r^{-1}, the inverse of the frequency of the initial rotation.

The remaining two-dimensional calculations were performed for 500-particle systems which have an initially uniform circular distribution in x-y space and zero thermal velocity. The evolution of such systems is then studied for various values of initial solid-body rotation. The initial positions are obtained by using a random number generator which gives a nearly uniform distribution over a circular region of the x-y plane.

We first present the results for the case where the frequency of rotation, ω_r, equals ω_g, the frequency required such that the centrifugal force balances the gravitational force. Thus,

$$\omega_r = \omega_g = \sqrt{2\pi G\rho} \tag{17}$$

where ρ is the mass density of the rods per unit length. The resulting evolution of the system is shown in figure 14. The time has been normalized to ω_g^{-1}. Figure 14 shows that the system is relatively stable. At $g = 6.32\omega_g^{-1}$ there appear four irregular spiral arms. However, at a later time the spiral

arms almost completely disappear and the system takes an appearance reminiscent of an elliptical galaxy.

The results for the case of zero initial rotation are presented next. Figure 15 shows that after an initial implosion the system expands and presents some highly irregular filamentary structure. After a second implosion the temperature of the system increases due to the randomness of the initial positions. The pressure due to the temperature then tends to reduce the oscillations and the system again takes a form similar to an elliptical galaxy.

For $\omega_r = \frac{1}{2}\omega_g$ the system again contracts initially and then expands. The results are shown in figure 16. An irregular structure appears initially which tends to disappear at a later time. Also at time $t = 4.2\omega_g^{-1}$ the system is clustered into two aggregates which combine again at a later time.

In figure 17 the results for the case $\omega_r = 1.3\omega_g$ are shown. The system pulsates and shows some irregular structure. The general behavior is very similar to that of the previous case for $\omega_r = \frac{1}{2}\omega_g$. The results for the two-dimensional stellar system are of a preliminary nature and additional work is required to investigate the evolution for systems with larger numbers of "stars."

REFERENCES

1. Lecar, M.: Validity of the Self-Consistent Collisionless Boltzmann Equation for a One-Dimensional Self-Gravitating Gas. Paper presented at the Fourteenth International Astrophysical Symposium, University of Liege, Belgium, June 1966.

2. Ford, J.: Approach of One-Dimensional Systems to Equilibrium. Phys. Rev., vol. 112, no. 5, pp. 1445-1451, Dec. 1, 1958.

3. Hohl, F.; and Feix, M. R.: Numerical Experiments with a One-Dimensional Model for a Self-Gravitating Star System. Astrophys. J., vol. 147, no. 3, pp. 1164-1180, Mar. 1967.

4. Hohl, F.: Collective Effects in Stellar Dynamics and Plasma Physics. Ph. D. Thesis, College of William and May, Williamsburg, Va., 1967.

5. Hockney, R. W.: Gravitational Experiments with a Cylindrical Galaxy. Paper presented at the Symposium on Computer Simulation of Plasmas and Many-Body Problems, College of William and Mary, Williamsburg, Va., Apr. 1967.

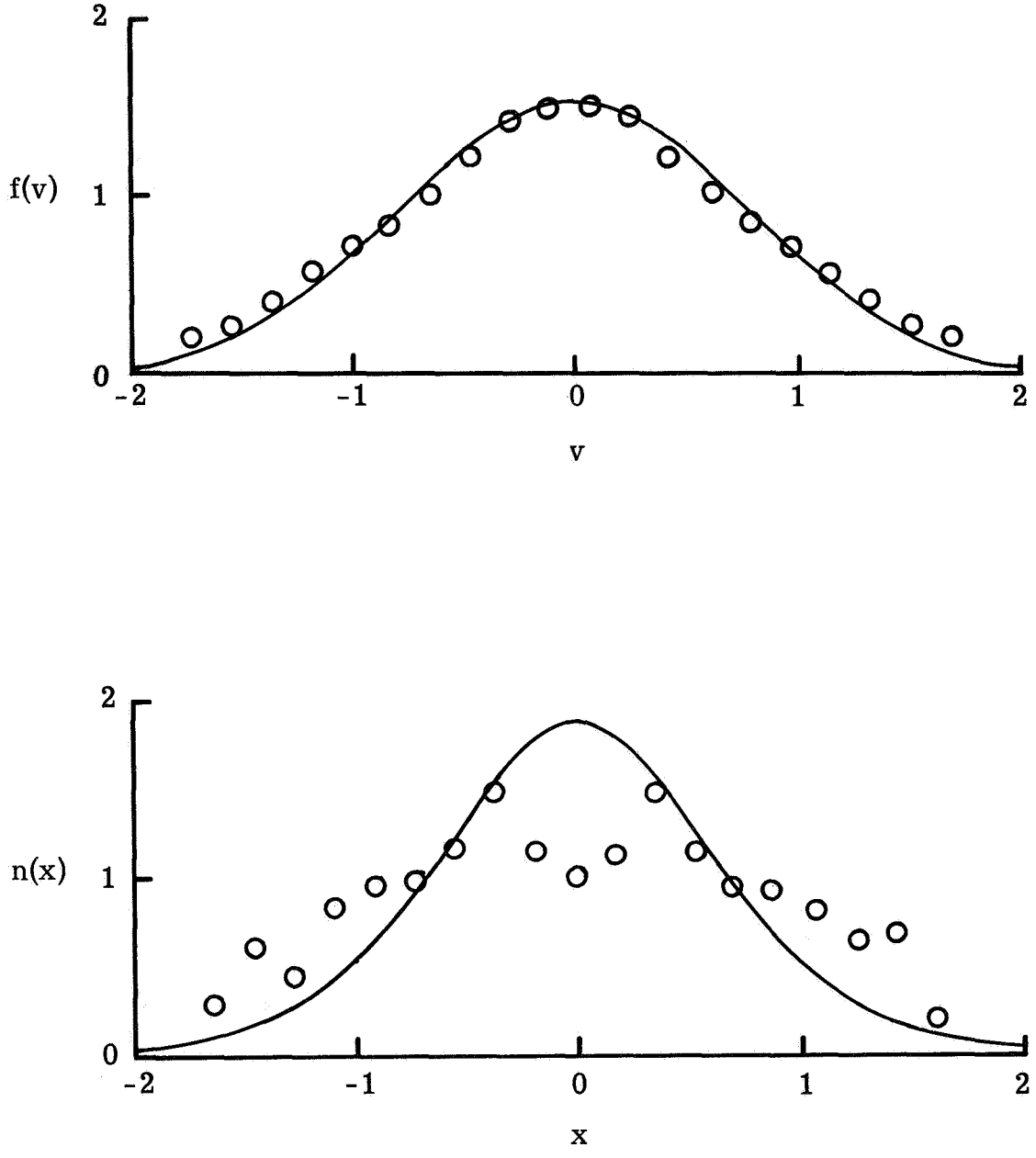

Figure 1.- Time-averaged velocity distribution and density for a 3-particle system.

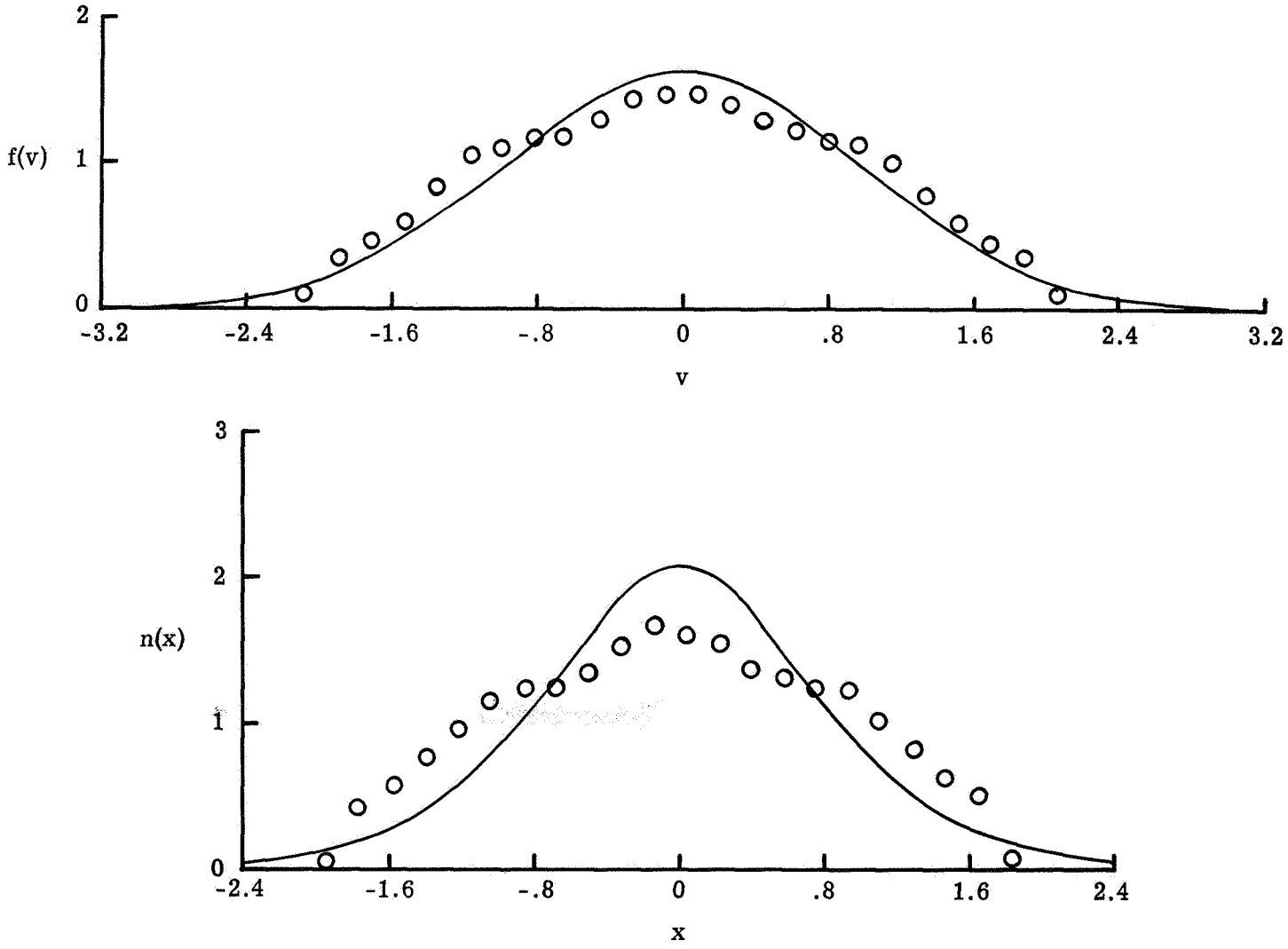

Figure 2.- Time-averaged velocity distribution and density for a 4-particle system.

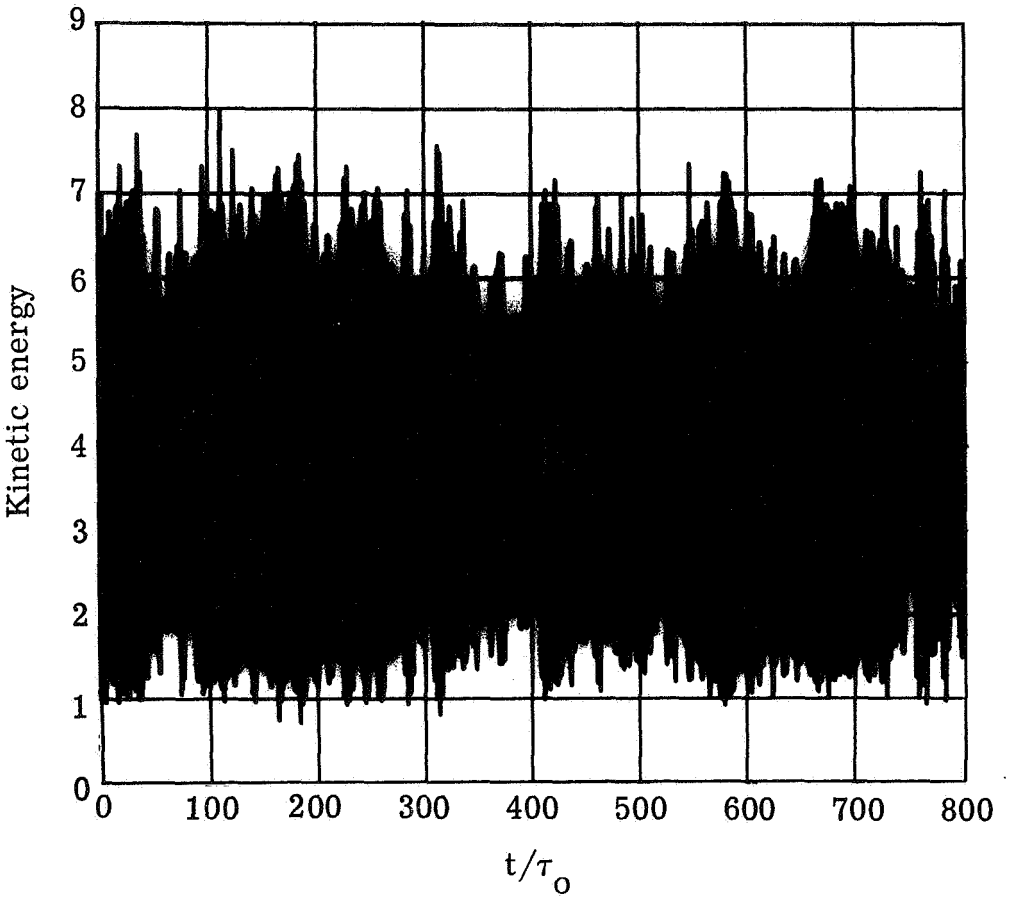

Figure 3.- Time variation of the kinetic energy for a 6-particle system.

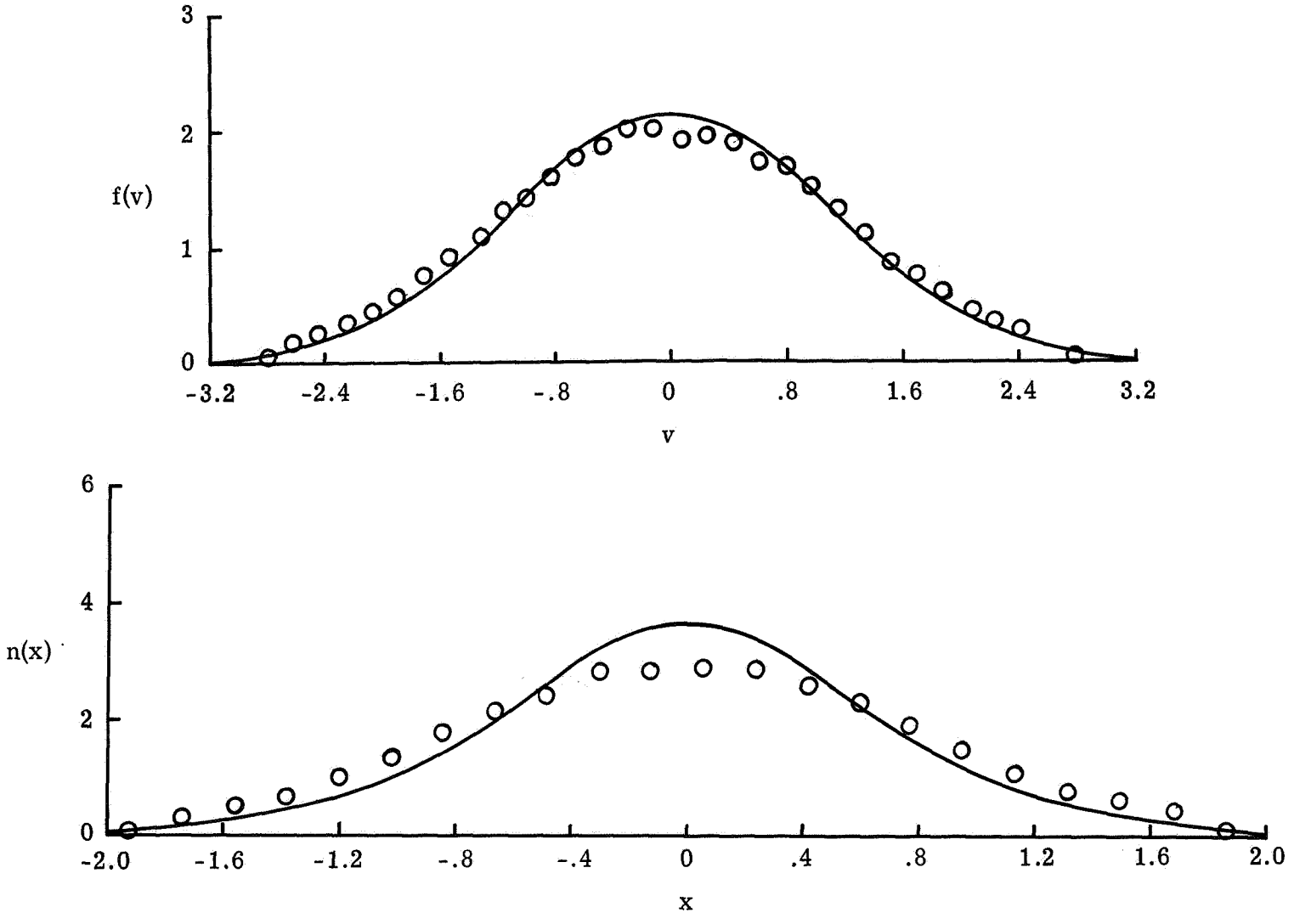

Figure 4.- Time-averaged velocity distribution and density for a 6-particle system.

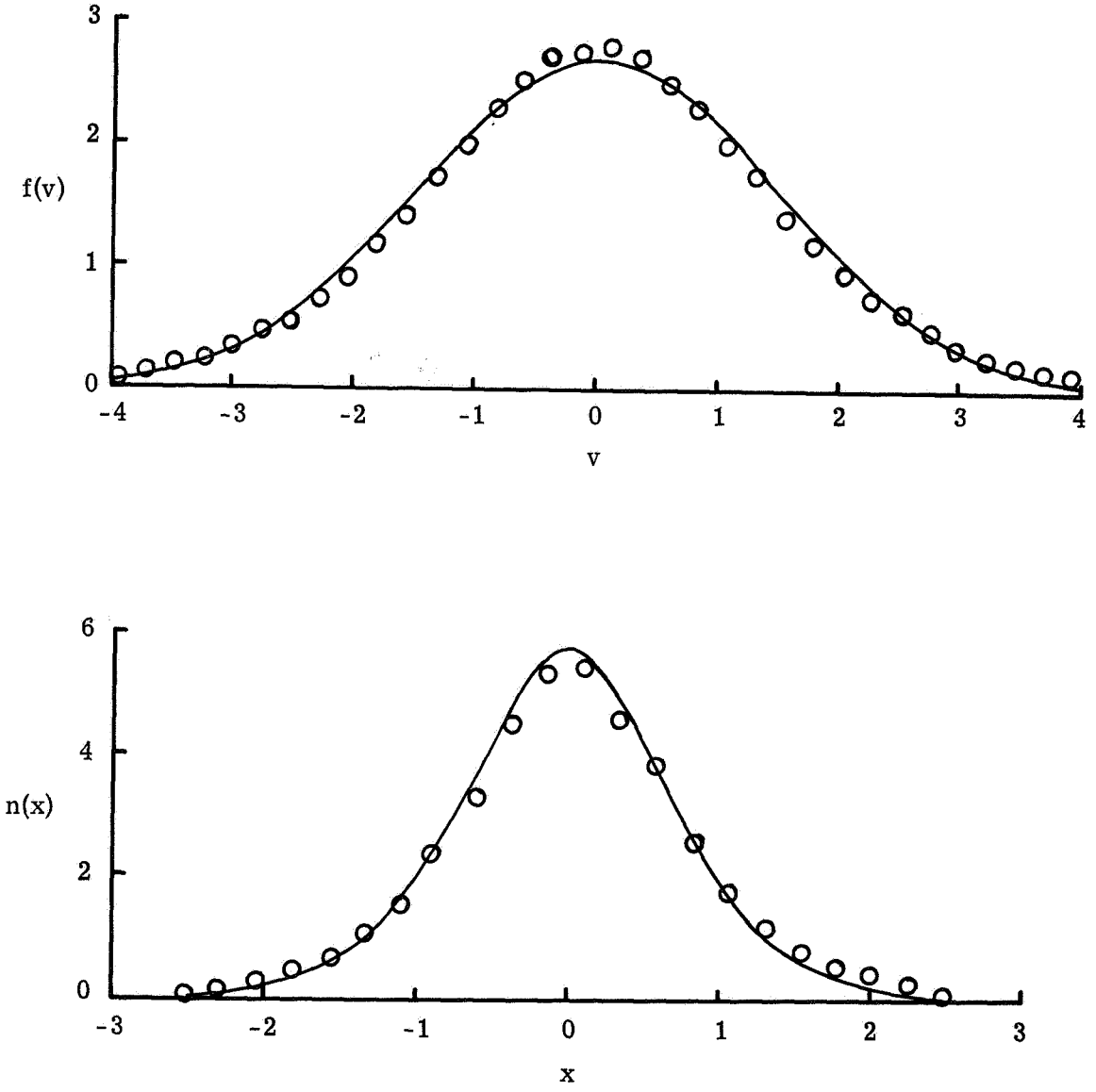

Figure 5.- Time-averaged velocity distribution and density for a 10-particle system.

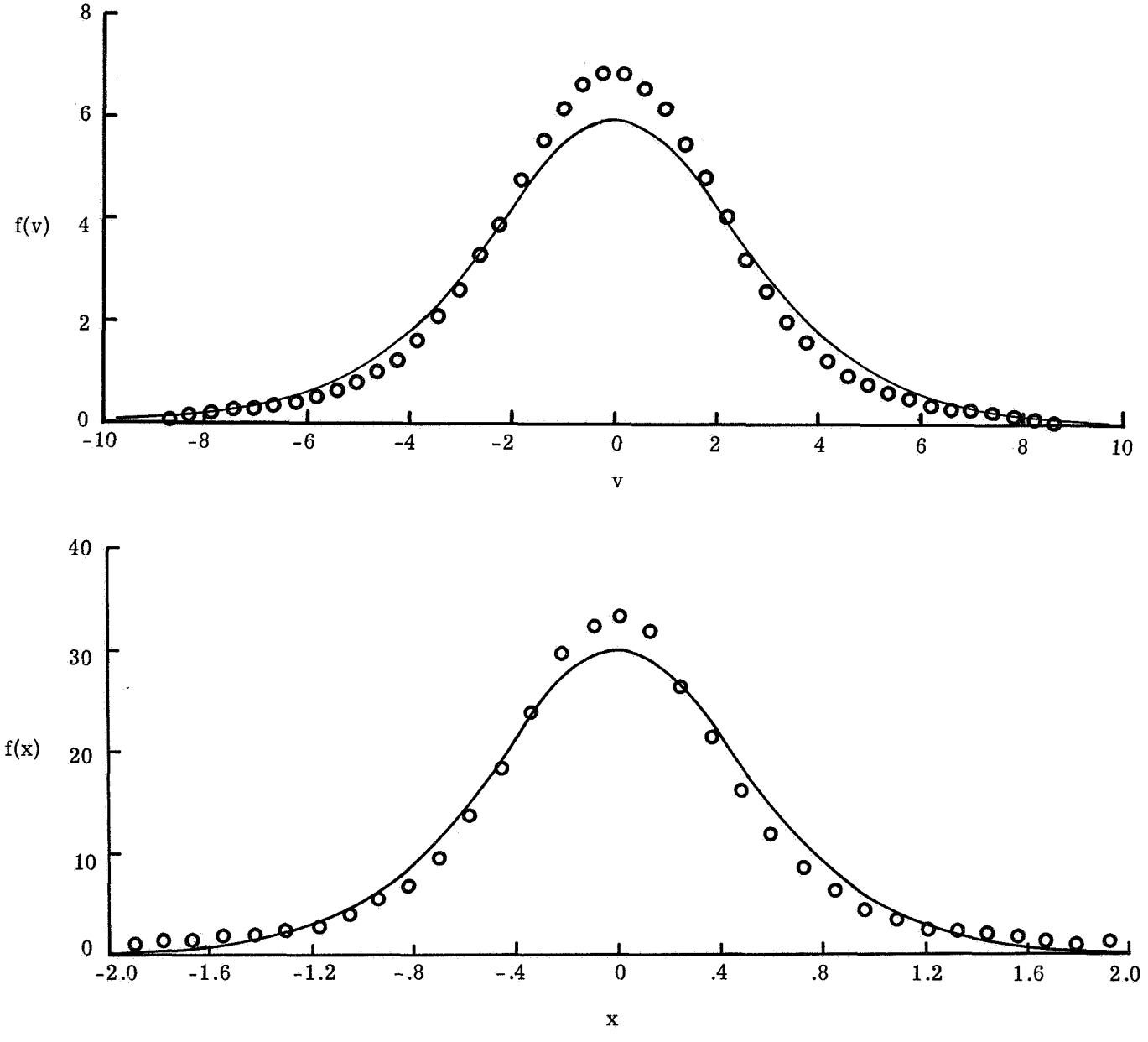

Figure 6.- Time-averaged density and velocity distribution for a 40-particle system.

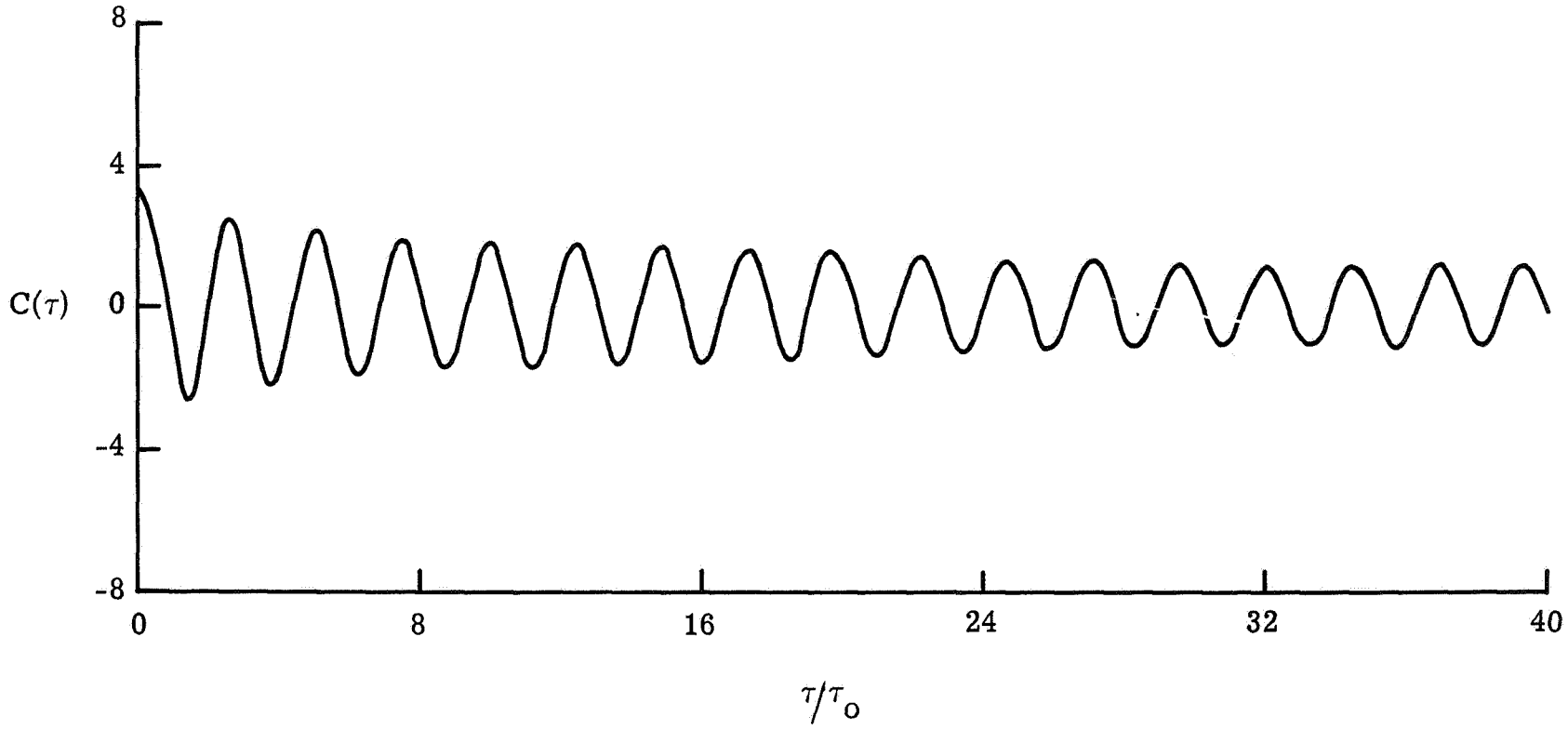

Figure 7.- Energy correlation function for a 6-particle system averaged over $20N^2$ periods.

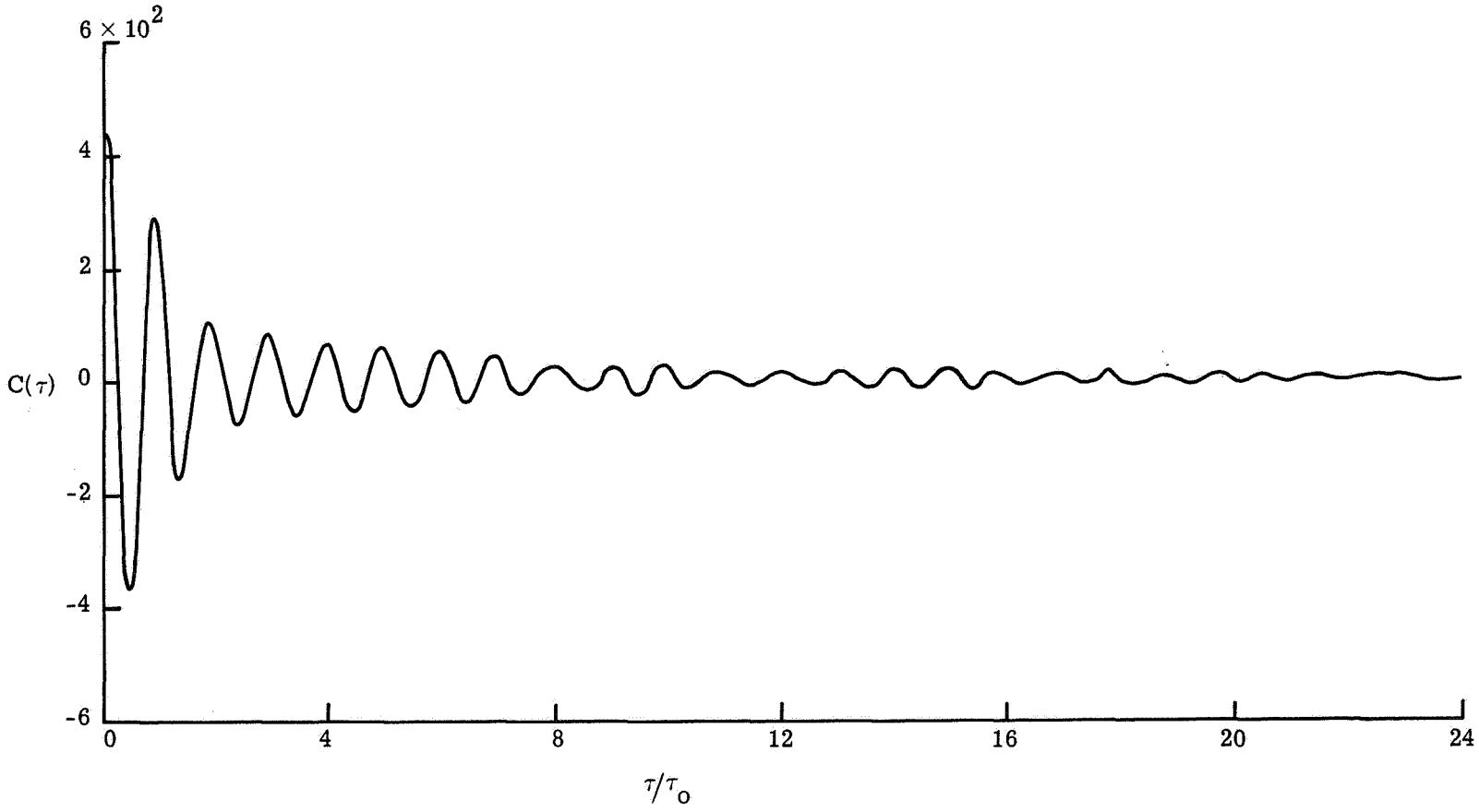

Figure 8.- Energy correlation function for a 40-particle system.

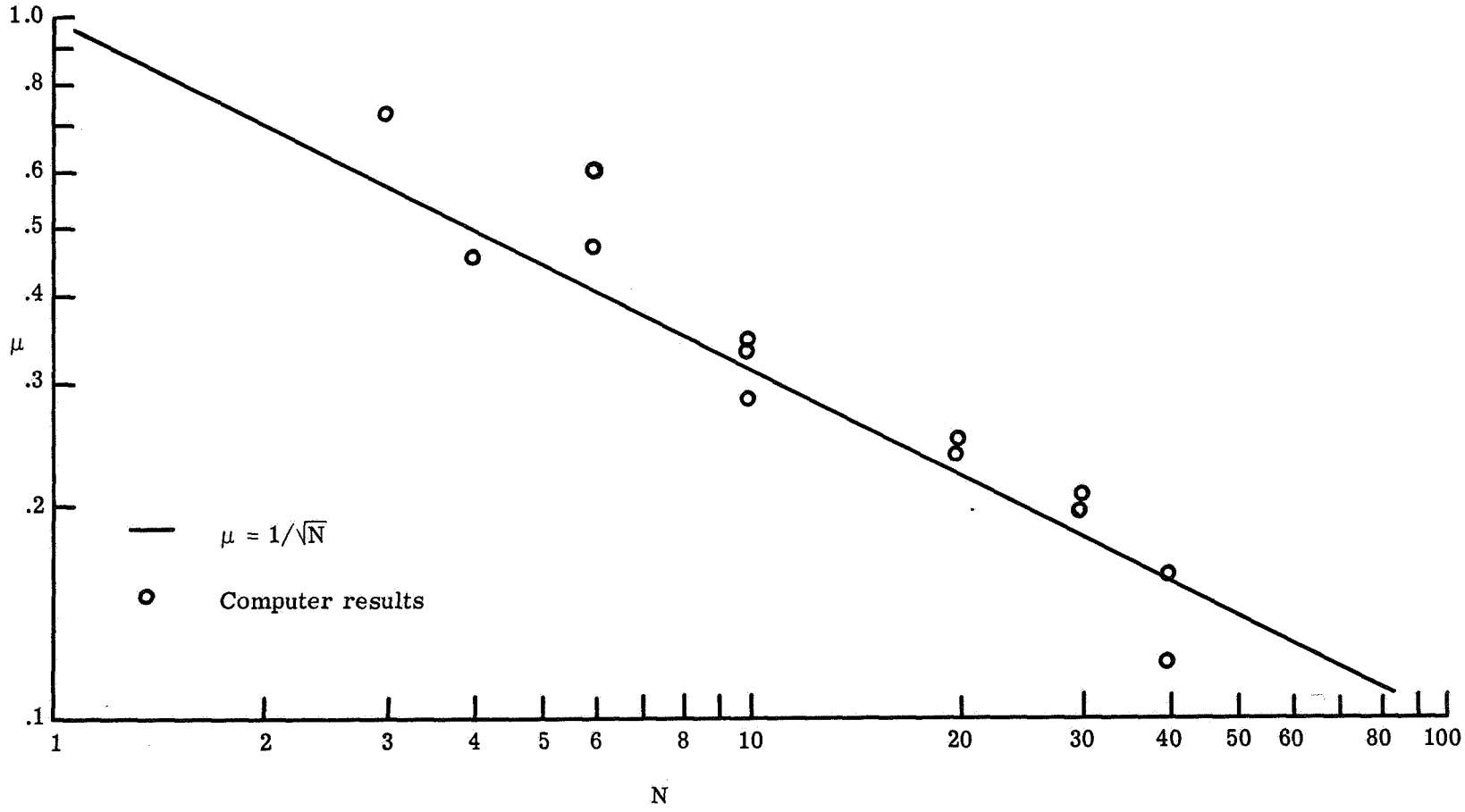

Figure 9.- Fluctuation in kinetic energy of the system as a function of the number of particles.

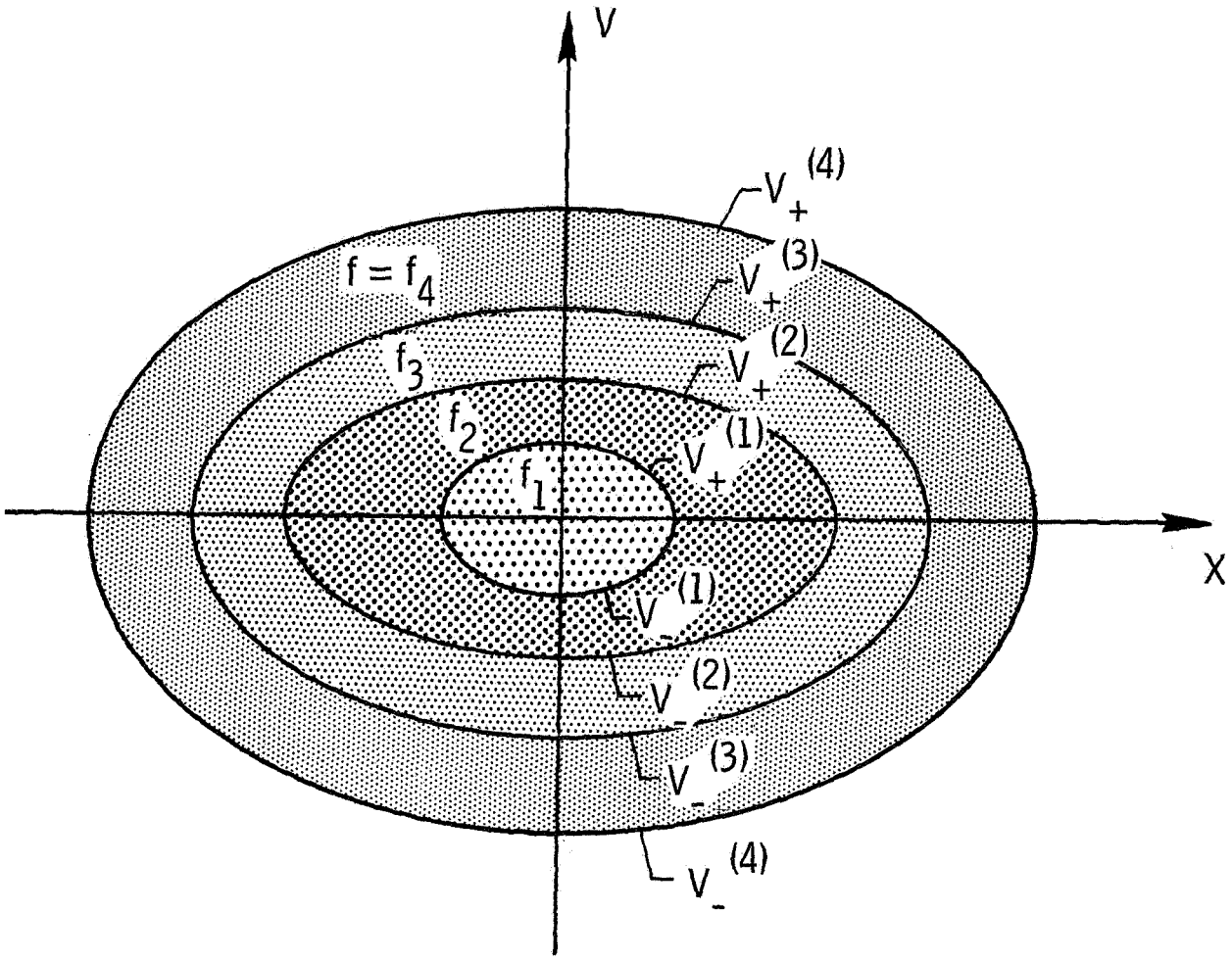

Figure 10.- Illustration of a multiple-contour water-bag distribution.

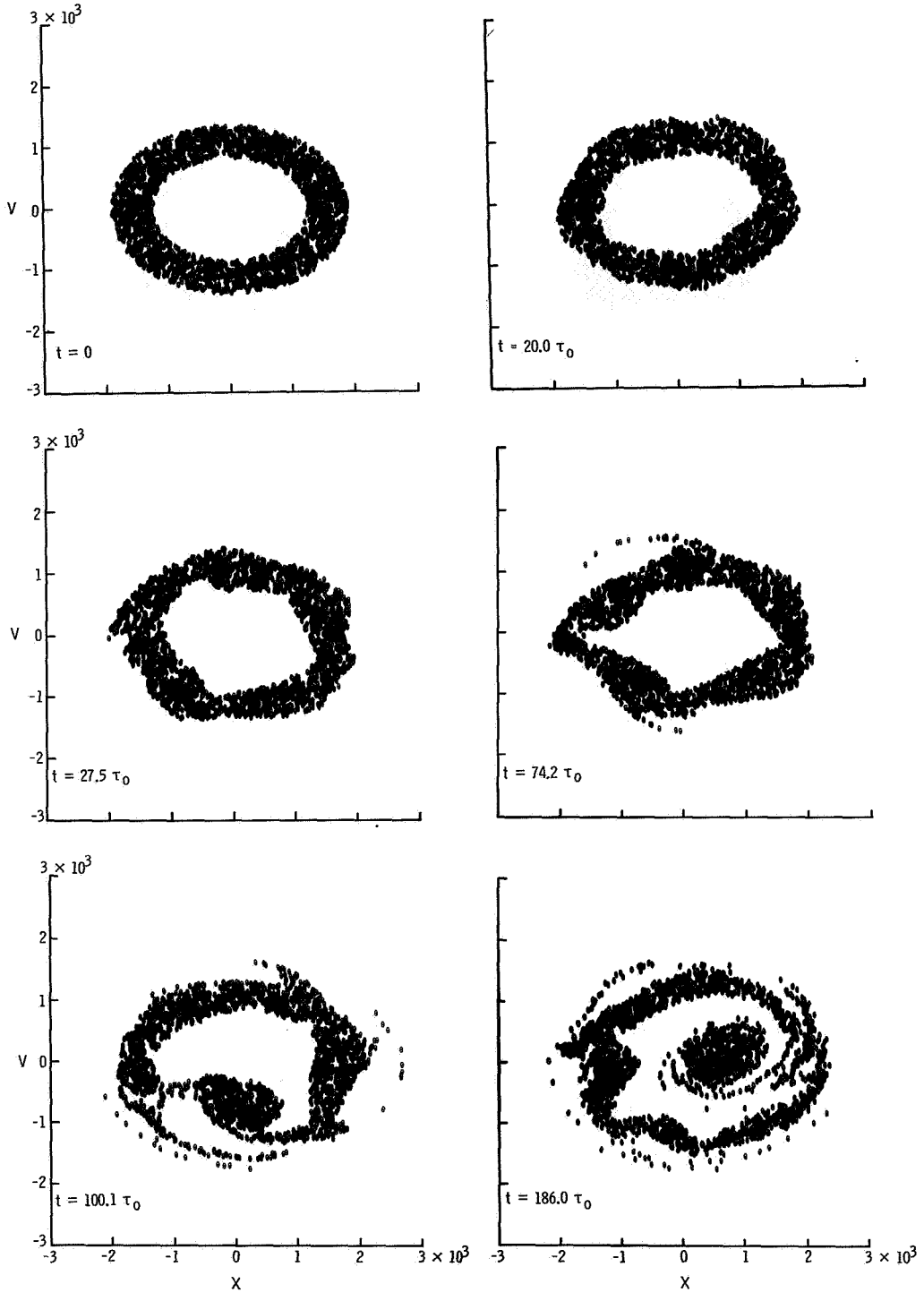

Figure 11.- Illustration of the time development of an unstable 2-contour system with $\nu = 0.4$.

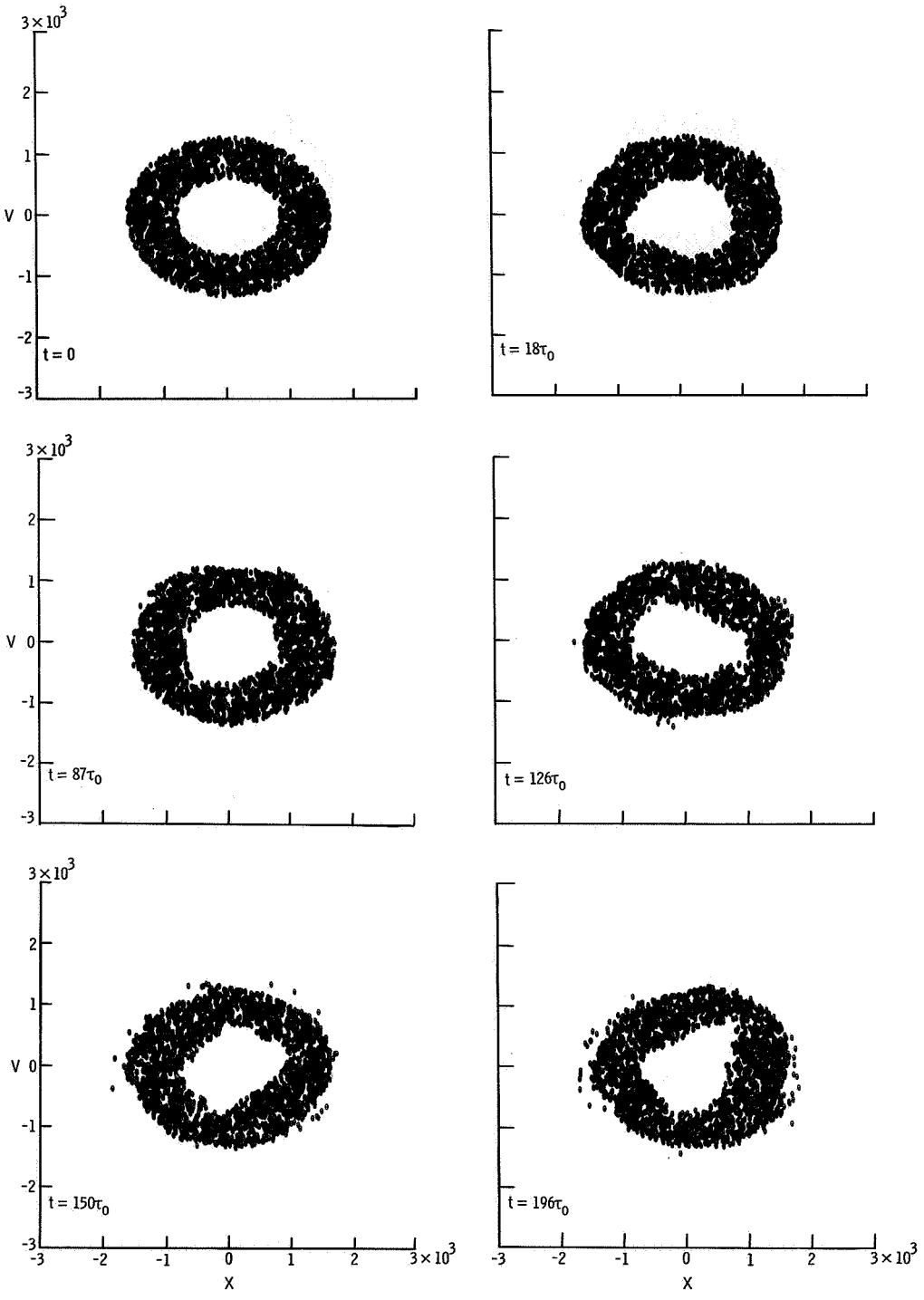

Figure 12.- Illustration of the time development of an unstable 2-contour system with $\nu = 0.25$.

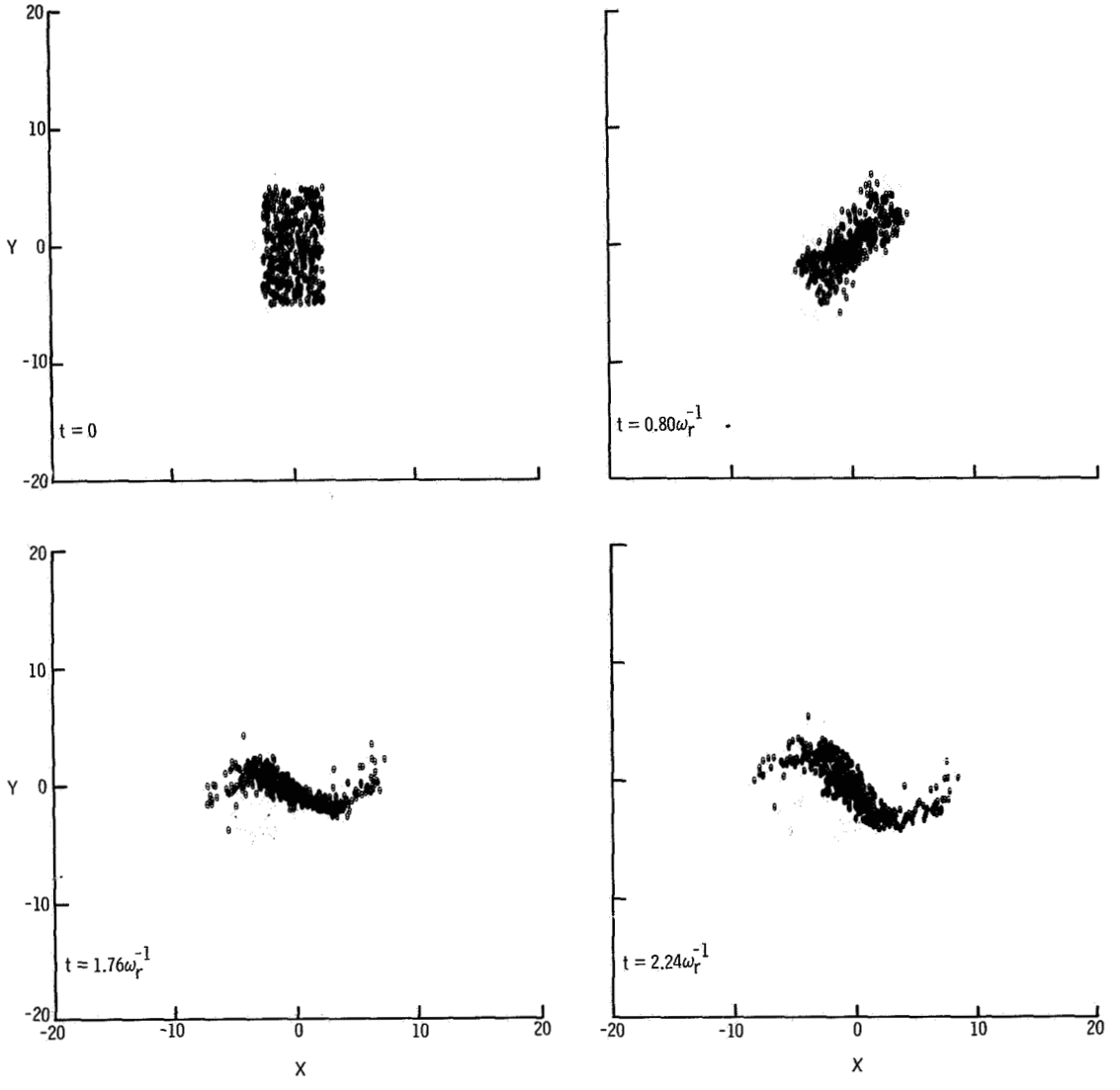

(a) Evolution up to $t = 2.24\omega_r^{-1}$.

Figure 13.- Time development of a stellar system of 400 mass rods.

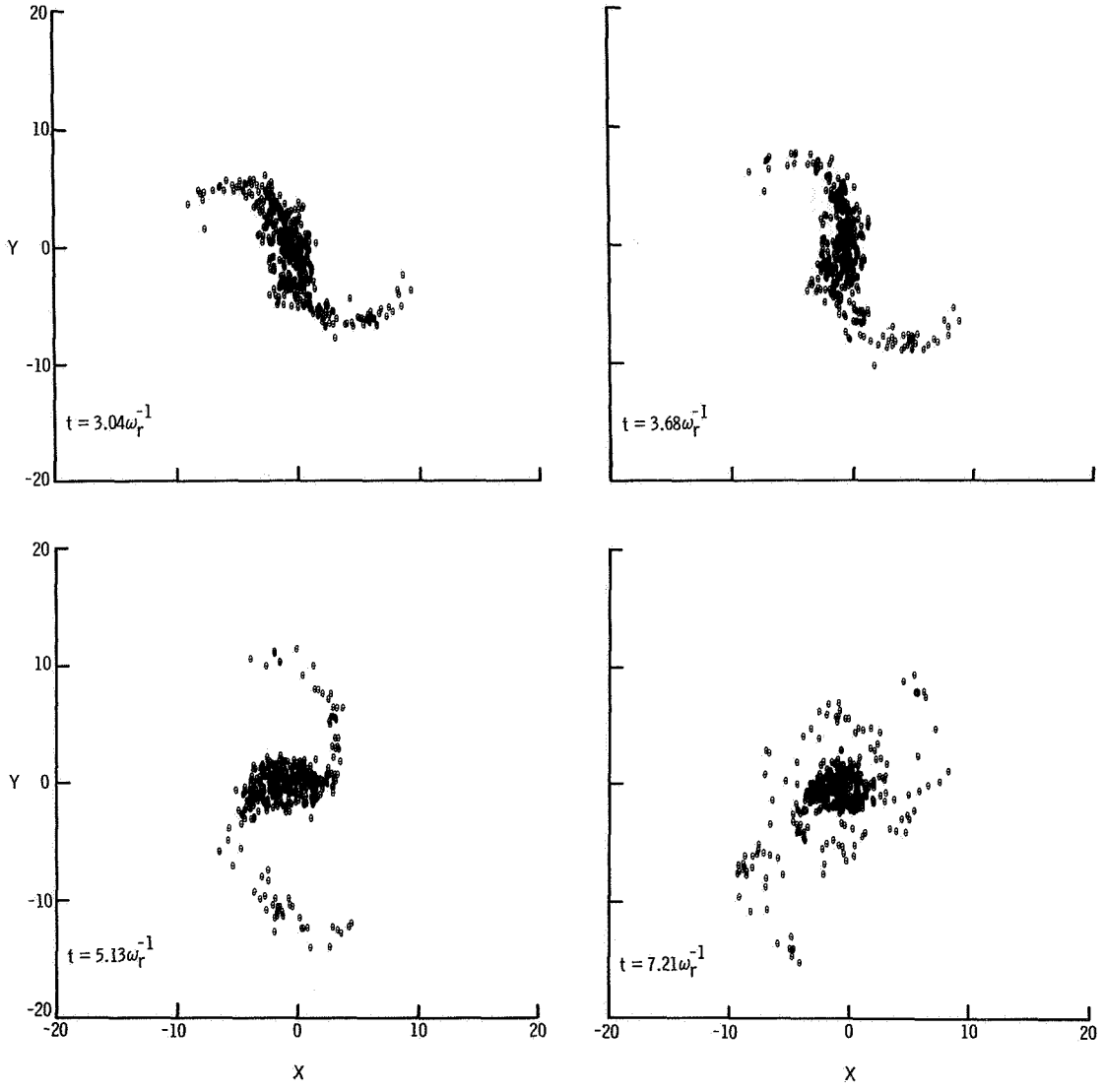

(b) Evolution up to $t = 7.21\omega_r^{-1}$.

Figure 13.- Concluded.

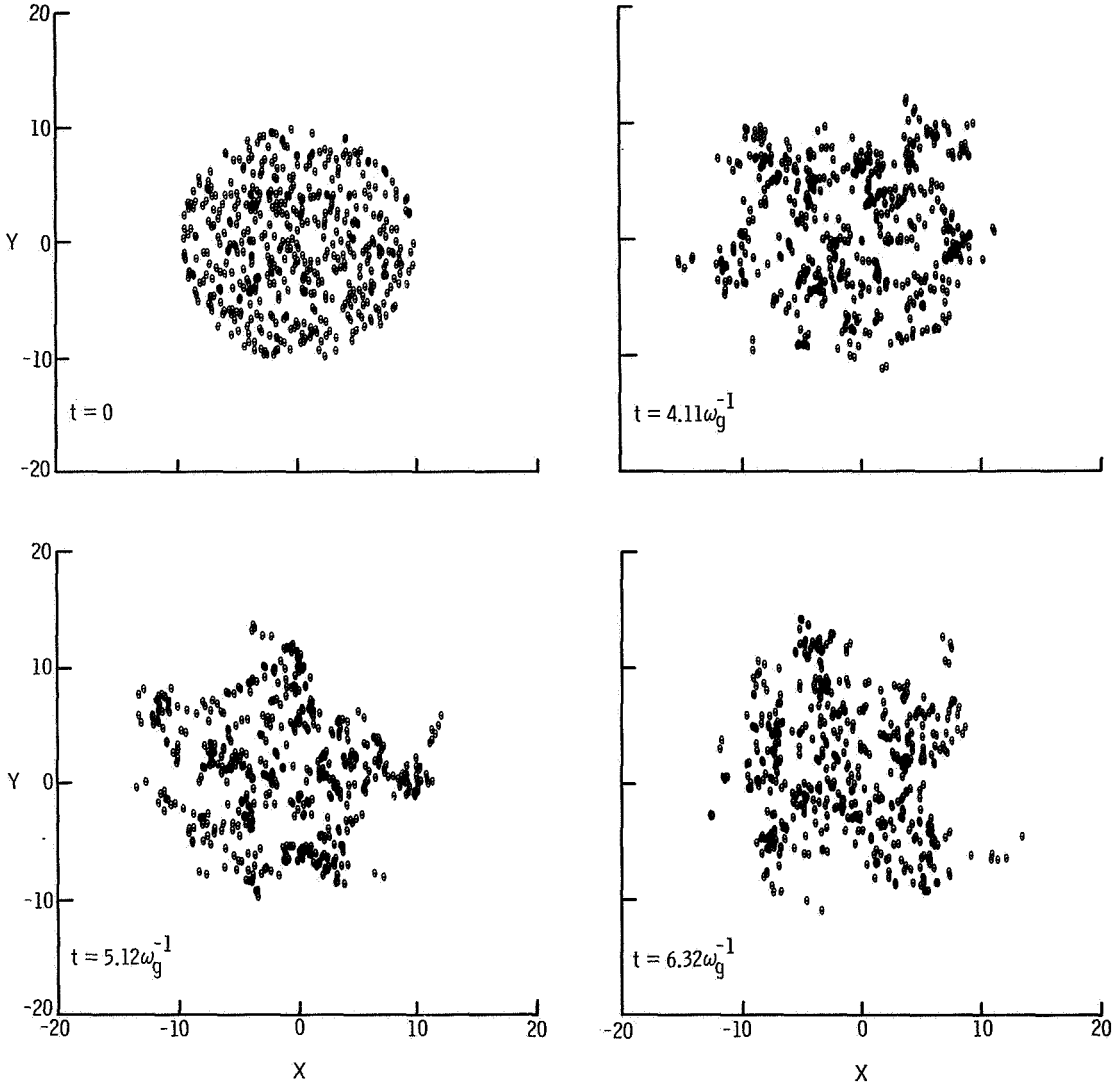

(a) Evolution up to $t = 6.32\omega_g^{-1}$.

Figure 14.- Evolution of a cylindrical stellar system with $\omega_r = \omega_g$.

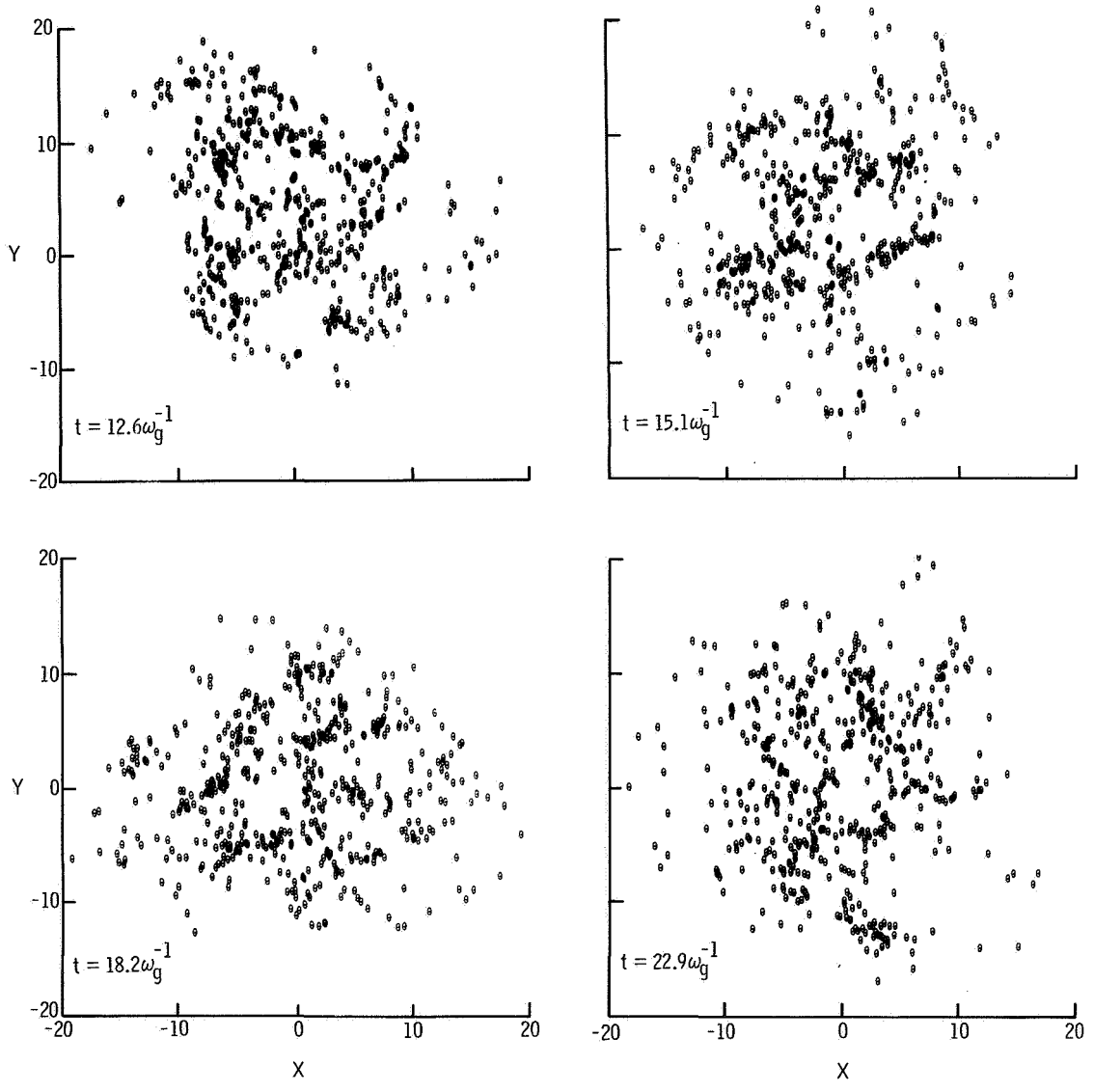

(b) Evolution up to $t = 22.9\omega_g^{-1}$.

Figure 14.- Concluded.

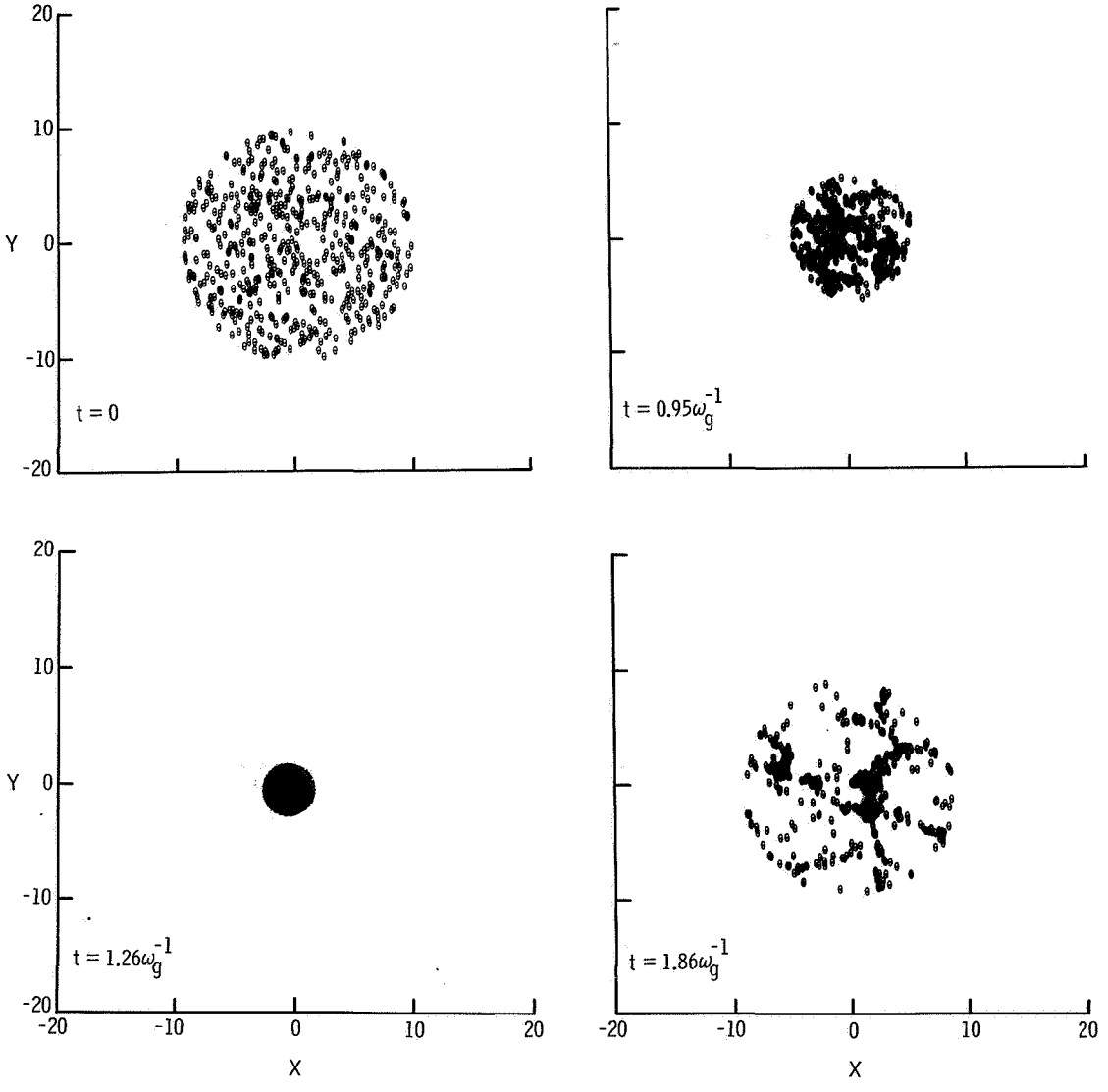

(a) Evolution up to $t = 1.86\omega_g^{-1}$.

Figure 15.- Evolution of a cylindrical stellar system with $\omega_r = 0$.

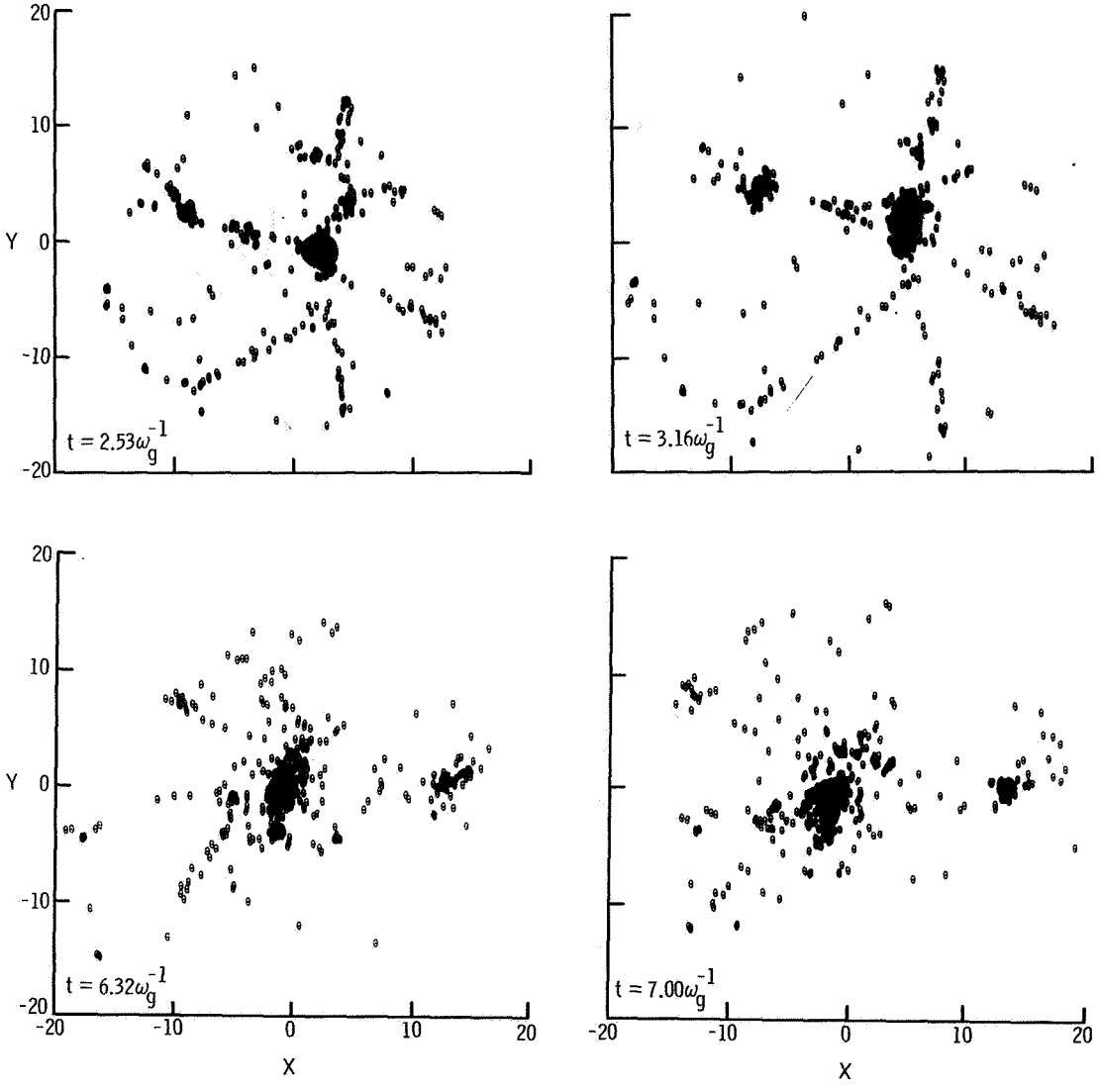

(b) Evolution up to $t = 7.00\omega_g^{-1}$.

Figure 15.- Concluded.

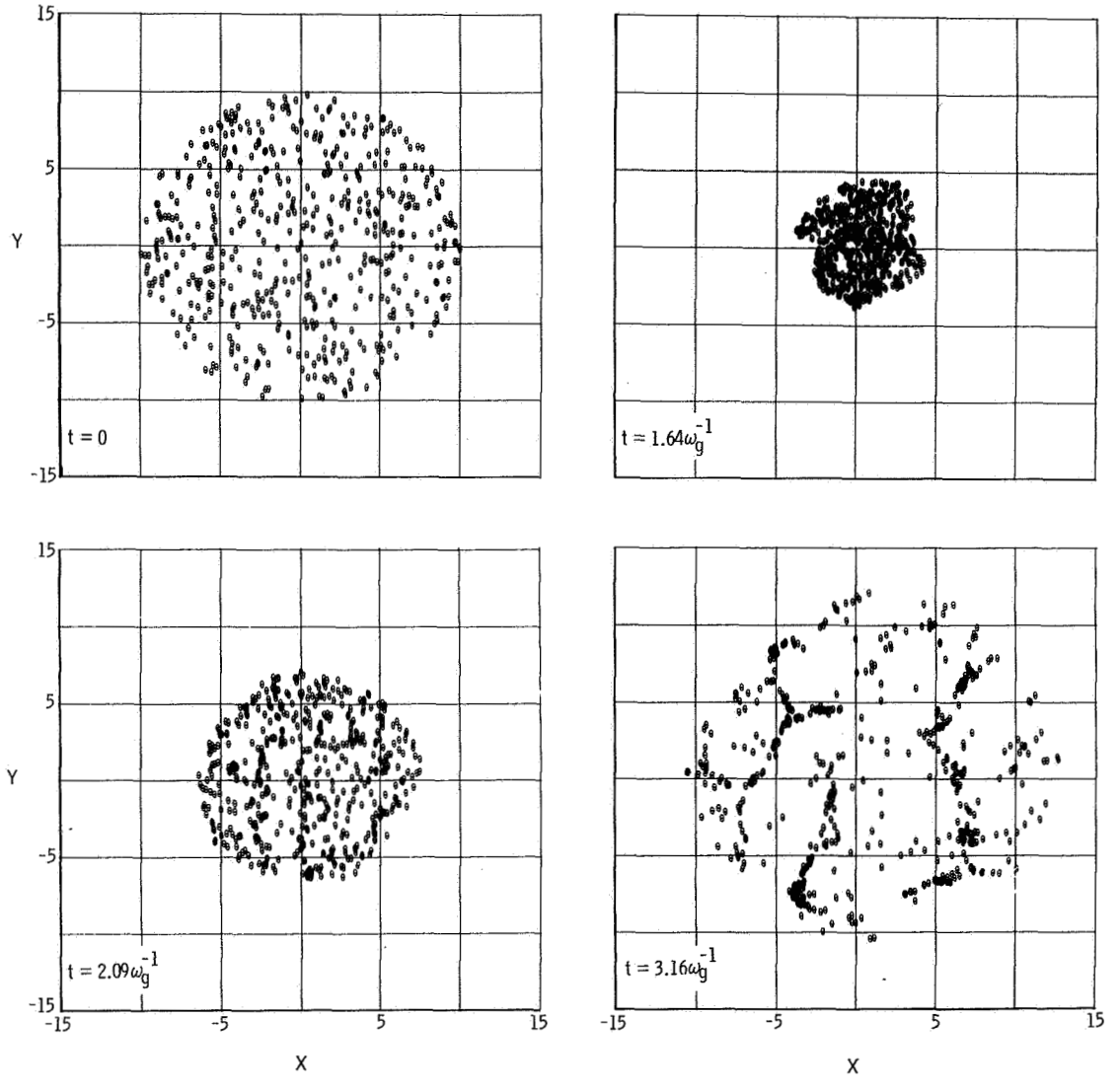

(a) Evolution up to $t = 3.16\omega_g^{-1}$.

Figure 16.- Evolution of a cylindrical stellar system with $\omega_r = 0.5\omega_g$.

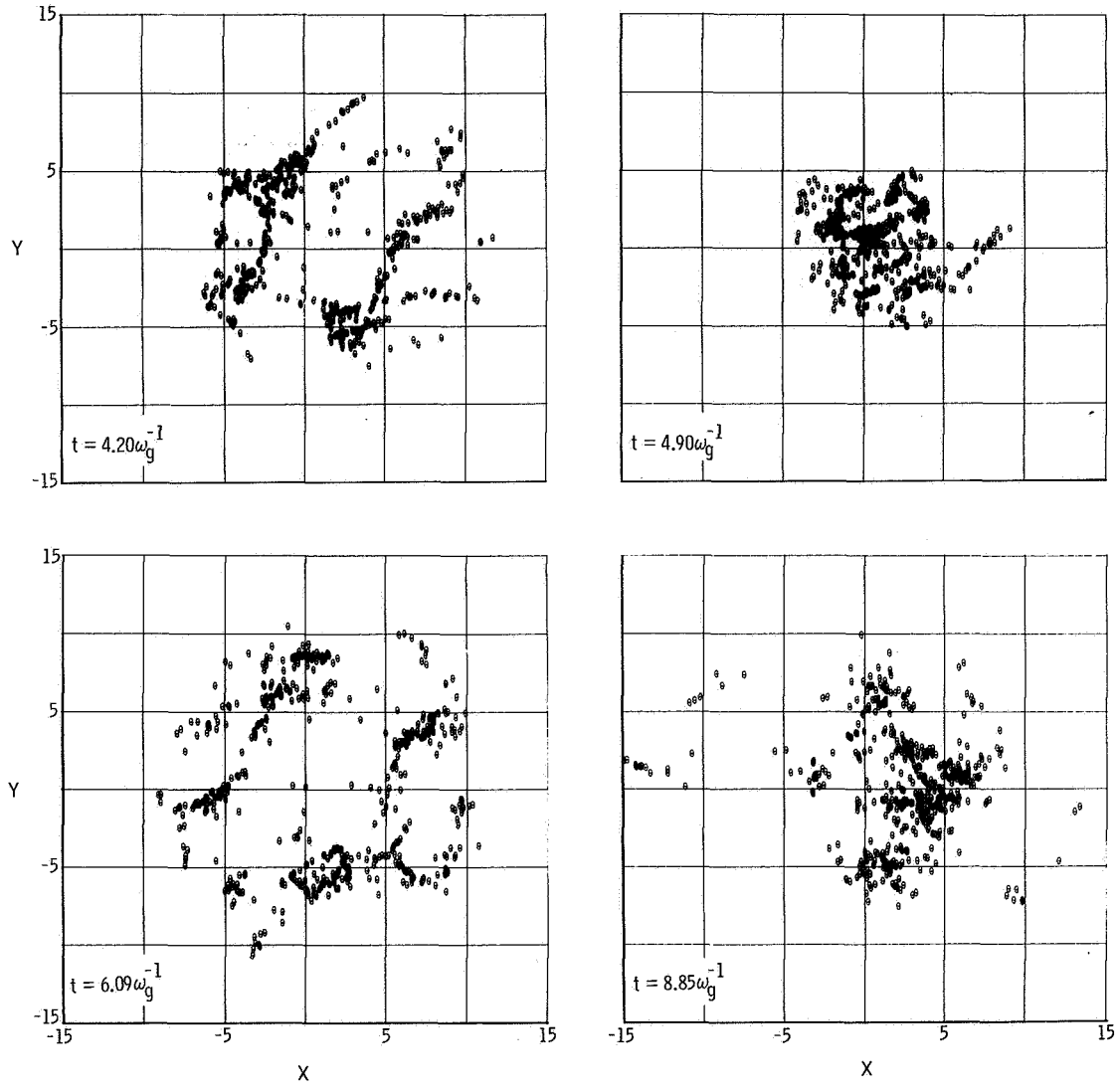

(b) Evolution up to $t = 8.85\omega_g^{-1}$.

Figure 16.- Concluded.

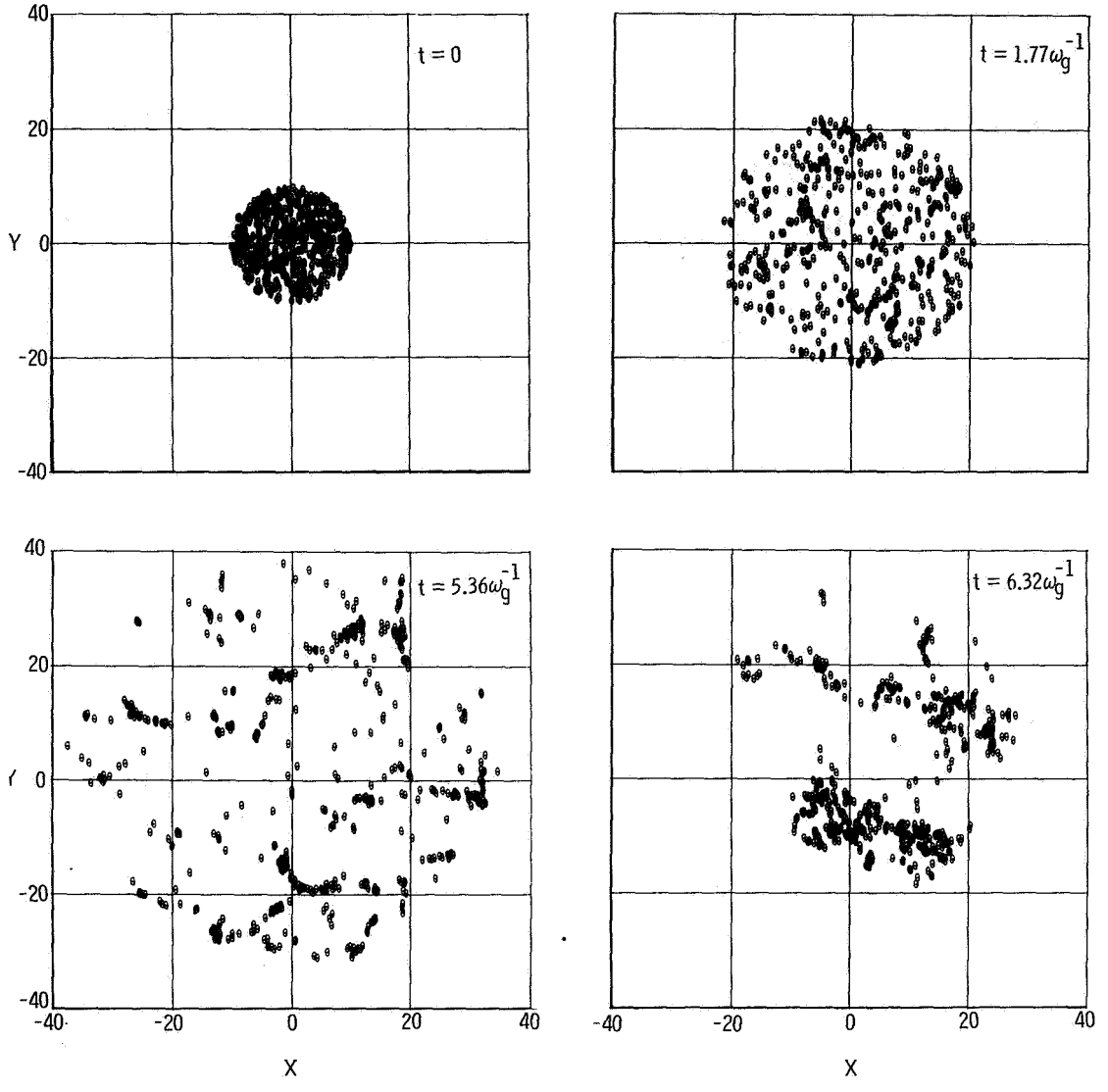

(a) Evolution up to $t = 6.32\omega_g^{-1}$.

Figure 17.- Evolution of a cylindrical stellar system with $\omega_r = 1.3\omega_g$.

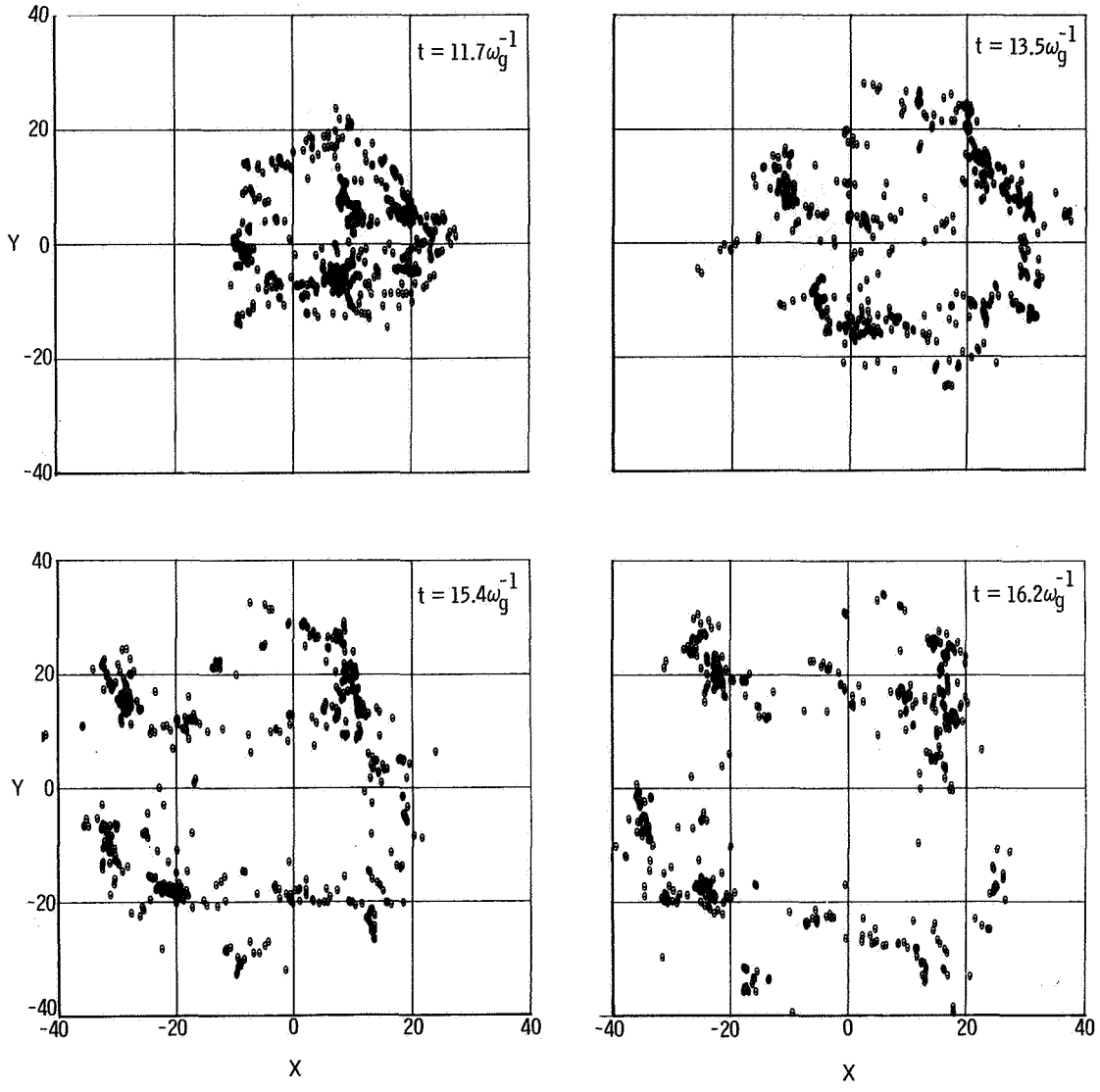

(b) Evolution up to $t = 16.2\omega_g^{-1}$.

Figure 17.- Concluded.

NASA-Langley, 1967